Thermal impact of Saharan dust over land. Part I: Simulation

Guy Cautenet, Michel Legrand, Sylvie Cautenet

Thermal Impact of Saharan Dust over Land. Part I: Simulation

GUY CAUTENET,* MICHEL LEGRAND,** AND SYLVIE CAUTENET*

Laboratoire de Physique de l'Atmosphère, Université Nationale, Abidjan, Côte d'Ivoire

BERNARD BONNEL AND GÉRARD BROGNIEZ

Laboratoire d'Optique Atmosphérique, Université des Sciences et Techniques de Lille Flandres Artois, Villeneuve d'Ascq, France

(Manuscript received 7 May 1990, in final form 19 July 1991)

ABSTRACT

Simulations are carried out to verify a mesoscale model in order to perform sensitivity tests of satellite response to atmospheric dust content. The model chosen is the mesoscale model of Colorado State University with a modified radiation parameterization in order to take atmospheric dust content into account. Downward and upward longwave irradiances are estimated using a 25-interval model. The shortwave part of the spectrum is processed by a very fast, highly parameterized, single-interval code. Tests using experimental data gathered during the Etude de la Couche Limite Atmosphérique Tropicale Sèche (ECLATS) experiment performed during the 1980 dry season near Niamey (Niger, West Africa) prove that dust content is satisfactorily handled. Three 24-h simulations performed under various meteorological and turbidity conditions show that ground surface energy exchanges are satisfactorily described, so that surface temperature is predicted with a standard deviation of about 1°C. Vertical profiles of computed air temperature and shortwave and longwave irradiances are also realistic.

1. Introduction

Dust clouds originating from Saharan sources are a prominent feature of the climate of the desert and its bordering regions, such as Sahel. Because of their high frequency of occurrence, their climatological influence is significant for these areas. They modify the radiative energy pattern in the atmosphere: observations of a thermal impact have been reported by several authors including Brinkman and McGregor (1983), Cerf (1985), D'Almeida (1986), and Legrand et al. (1988). Therefore, satellite remote sensing of dust may be possible provided that a relation between the upward longwave irradiance at the top of the atmosphere and the tropospheric aerosol characteristics is clearly and unequivocally substantiated. Tanré and Legrand (1991) described a method for the retrieval of the aerosol optical depth using IR satellite imagery. For the development of such methods, however, it is necessary to first determine the effect and the relative importance of the various factors that have an impact on the satellite response.

The mechanisms governing the thermal impact of the dust in the earth–atmosphere system are hereafter qualitatively described. The dust absorbs and scatters both shortwave and longwave radiations, and it also emits longwave radiation. These processes result in the attenuation of the downward shortwave radiation, chiefly by scattering, and in the increase of the downward longwave radiation, by addition of the dust thermal emission. The total downward irradiance incident onto the ground is reduced during the daytime, because the attenuation of the shortwave component overcompensates the increase of the atmospheric irradiance. On the other hand, the longwave irradiance is increased during nighttime.

These modifications lead to a shift of the energy balance at ground, with a redistribution among the radiative and nonradiative components, implying a change of the turbulent energy transfer in the lower troposphere. As a consequence, the thermal impact is located primarily at the ground surface. The presence of dust induces a fall of the ground surface temperature during daytime, and a rise during nighttime. Furthermore, the temperature of the lower troposphere is modified because dust induces a spatial redistribution of the physical properties of the turbid medium and a modification of the profiles of the radiative (longwave and shortwave) and turbulent fluxes. It follows that the heating

* Present affiliation: Laboratoire Associé de Météorologie Physique, Université Blaise Pascal, Clermont-Ferrand, France.

** Present affiliation: Laboratoire d'Optique Atmosphérique, Université des Sciences et Techniques de Lille Flandres Artois, Villeneuve d'Ascq, France.

Corresponding author address: Dr. Guy Cautenet, Laboratoire Associé de Météorologie Physique, Université de Clermont II, 12 Avenue des Landais, 63000 Clermont-Ferrand, France.

rates, originating from the divergence of the radiative and turbulent fluxes, are also modified.

This qualitative and somewhat approximate description obviously shows the intricacy of the interacting mechanisms. This complexity could lead to the questioning of the general applicability of an IR method of aerosol remote sensing. Conversely, if we can show that all the important factors can be identified and their effect controlled, such a method becomes possible. Thus, we have to answer the following questions. What are the parameters (radiative and nonradiative) that have a significant impact on the satellite response, and what is their sensitivity? How do the nonradiative processes interact and what is their real impact? Two ways are possible: either (i) the use of large sets of experimental data (from ground surface, atmosphere, and satellite) corresponding to diversified conditions for the Sahelian and Saharan zones, or (ii) the attempt to compensate the lack of experimental data by numerical simulation. At present, experimental data are very scarce; thus, we are in the second case. It is clear that this study could be achieved only by using a sophisticated model.

Earlier simulations of the radiative effects of the aerosol and of its thermal consequences have been carried out chiefly in order to obtain global aerosol climatic impact estimates. A detailed review of such studies is presented by Lenoble (1984). In this prospect, Joseph (1977), and more recently Tanré et al. (1984) and Coakley and Cess (1985), using general circulation models, have reported results that suggest a significant role of the desert aerosol in climatic change of the concerned areas.

Part I of this paper deals with the study of the impact of desert aerosol during the whole daily cycle, from the simulations obtained using a mesoscale boundary-layer model. In section 2 the model used is presented and modifications, added for a careful processing of the radiation parameterization, are described. Section 3 is devoted to the checking of the modified model by comparison of computed results with the experimental dataset issued from the ECLATS experiment (Druilhet and Tinga 1982) implemented in the Sahelian area during the dry season (Niamey, Republic of Niger; November–December 1980).

Part II (Legrand et al. 1992) is an application of Part I, relating to the satellite remote sensing of dust over Africa using the 10.2–12.5-μm channel of Meteosat. The aim is to determine the sensitivity of the satellite response to various physical variables, in order to define a relevant parameterization for the retrieval of the aerosol optical depth using satellite imagery (Tanré and Legrand 1991).

2. The numerical model

a. The mesoscale model

We choose a two-dimensional (2D) version of the Colorado State University (CSU) mesoscale model. A 2D version is preferable whenever horizontal inhomogeneities are assumed to be small. This boundary-layer model has been described in earlier papers (Mahrer and Pielke 1978). Many authors used it for numerical simulations of mesoscale phenomena in various regions of the world. In West Africa, it was recently operated to investigate the sea-breeze interaction with synoptic circulation (Cautenet and Rosset 1989). It has been used to describe the behavior of a heated planetary boundary layer (PBL) in the Wangara experiment (Pielke and Mahrer 1975) in a 2D version. As far as we know, this model has not yet been tested under Sahelian tropical conditions, where superadiabatic situations are frequently observed. In this model, hydrostatic and barotropic approximations are assumed. The model calculates horizontal wind speed, potential temperature, and specific humidity on an uneven grid step. The growth of the planetary boundary layer is described using Deardorff's prognostic equation (1974).

The orientation of the model is west–east for the x axis, and south–north for the y axis [the intertropical discontinuity (ITD) was located 200 km south of the experimental site so that the wind hodograph recorded during this period showed that the prevailing wind (Harmattan) was in the eastern sector]. According to the 2D assumptions, all the model variables are independent of y. The vertical steps increase with the height: 2, 10, 100, 300, 700, 1200, 2000, 3000, 4000, 5000, and 6000 m. The horizontal extent of the model consists of 21 grid steps equally spaced (a horizontal grid step is 20 km). A soil description is included to allow an estimate of the surface temperature, which leads to an estimate of the surface energy budget through an iterative process. In order to account for the large temperature gradients that are likely to exist just below the ground surface in dry Sahelian regions, we have slightly modified the soil grid, allowing an exponential expansion: the first step is 1 cm, and the last one is 30 cm. The lowest level is about 1 m deep. The surface energy budget is described completely. The model results at the center of the domain are displayed in order to be compared with the experimental data: wind speed, temperature and humidity profiles, upward and downward shortwave and longwave irradiance profiles. Symbols for irradiances are $F_s\uparrow$ (up) and $F_s\downarrow$ (down) in the shortwave spectrum, $F_l\uparrow$ and $F_l\downarrow$ in the longwave spectrum. A large set of additional surface data is also available: ground surface temperature T_S, turbulent sensible and latent heat flux densities H and LE, surface downward and upward longwave and shortwave irradiances, ground-conduction heat flux density G. No vegetation is taken into account. Horizontal homogeneity of surface and atmospheric properties is assumed.

Shortwave and longwave radiation computation schemes, in the initial model, do not account for the aerosol effects; thus, the main modification brought to the model deals with radiative transfer as described in the next section.

b. Modifications in radiation parameterization

The initial model includes a quite efficient radiation parameterization, but it is not adapted to our purpose because it does not take dust effect into account. It has been replaced by shortwave and longwave codes developed by the Laboratoire d'Optique Atmosphérique, Lille, France (LOA). The atmosphere is divided into 20 layers according to the vertical coordinate. Layers 1–11 correspond to the vertical distribution in the mesoscale model. Temperature, humidity, and pressure profiles used as input of the radiation subroutines are computed by the mesoscale model from ground level to level 11 (6000 m). They are held constant over 6000 m. Aerosol concentration and size are held constant throughout the day. The horizontal homogeneity of the aerosol properties is assumed.

The infrared code divides the spectrum into 25 intervals ranging from 4.5 to 250 μm. It was initially developed by Fravalo et al. (1981) and was adapted in order to describe the radiation interaction with clouds. Such a medium presents a large optical thickness so that scattering was resolved with the Eddington scheme. Fouquart et al. (1987b) developed a version allowing the use of the two-stream scheme in order to describe the aerosol effect (optical thickness close to unity). This model can simulate various cases of aerosol properties. The aerosol may be considered as gray, and the scattering may be neglected. This is the case in this paper for the comparison of computed results with the ECLATS experiment data, as aerosol studied during ECLATS could be considered as gray and nonscattering (Fouquart et al. 1987b). However, a nongray scattering aerosol can be taken into account by our codes. This is done in Part II, where the ECLATS effects are compared with a coarse-grained nongray scattering aerosol. The accuracy of this code was tested by comparing its results with issues of a narrow-band model (365 intervals): the underestimation in irradiance $F_l\downarrow$ at ground level by the 25-interval model is about 15 W m^{-2} for a clear atmosphere with nonscattering dust. This bias is due to the lesser spectral resolution and the error introduced by the transmittance calculation method. Moreover, using Eclats data of 26 November, the 25-interval model showed that neglecting aerosol scattering resulted in a very weak underestimation in $F_l\downarrow$ at ground level of about 1 W m^{-2} and had a negligible effect on radiative cooling. Thus, aerosol scattering may be disregarded in the ECLATS experiment: only absorption is considered, which saves computer time to some extent. Aerosol absorption itself is rather weak: the longwave optical thickness is typically 0.10 times the shortwave one (Fouquart et al. 1987b). So, it can be simply stated that the ECLATS aerosol is gray. Possible discrepancy arising from this assumption is obviously negligible when compared with the other errors, particularly with the effect of the width of the spectral intervals. Aerosol longwave absorption may thus be represented by a mean gray absorption coefficient per particle σ_l. In summary, using the 25-interval model with the two-stream approximation, added to the hypothesis of a gray aerosol without scattering, involves a total error of about 15 W m^{-2}, which is quite acceptable for the purpose of sensitivity tests. The bias is smaller on the computed upward irradiance $F_l\uparrow$ at ground level.

The shortwave part of the spectrum, that is, from 0.25 up to 4 μm, is described by a single interval model (Fouquart and Bonnel 1980). It accounts for gas absorption (water vapor, carbon dioxide, ozone) using spectrally averaged transmission functions in each atmospheric layer. The transfer equation in a scattering medium is resolved with an approximate method based upon a delta-Eddington scheme, sufficiently accurate when only irradiances are interesting. Aerosol properties are described merely with the help of three spectrally averaged parameters: the extinction coefficient σ_s (or the optical thickness $\delta_s = N\sigma_s$, with N being the number of particles per surface unit in a vertical column), the single-scattering albedo ω, and the asymmetry factor g. This code is very fast. Its accuracy has been tested against various reference models (Fouquart et al. 1990). Comparison tests between both models indicate a departure (overestimation) of 7 W m^{-2} or less, which proves the adequacy of the single interval model.

Finally, the presence of high clouds was obvious from surface pyrheliometric observations, but no measurement of the cloud cover was available. For this reason, we have considered two additional parameters: the shortwave and longwave optical thicknesses $\delta_s{}^c$ and $\delta_l{}^c$ associated with clouds introduced at the 7000-m level. Because of a lack of direct measurement, both have been determined by tuning (see section 3).

In summary, both radiation codes require profiles of air temperature and humidity, atmospheric pressure, and aerosol concentration (size distribution is independent of altitude in agreement with the results of the ECLATS experiment): all of them, except for the last one, are provided by the model itself at each time step. Moreover, longwave calculations require the gray absorption coefficient per particle σ_l and the longwave cloud optical thicknesses $\delta_l{}^c$, whereas the shortwave code requires the aerosol parameters δ_s (or σ_s), ω, and g, and the cloud parameter $\delta_s{}^c$. Solar irradiance S at the top of the atmosphere is calculated according to the date. For each level, irradiances divergence (shortwave and longwave) is derived from the above radiation calculations.

3. Results

a. Description of the experimental dataset

The ECLATS experiment took place in 1980 during the dry season in the Republic of Niger (West Africa) near Niamey (14°N, 2°E), in the Sahelian area. It was carried out jointly by French and African laboratories.

Its main purpose was the investigation of radiation effects on the boundary-layer dynamics. The period under study (November and December) is commonly associated with strong variations in atmospheric turbidity due to dust outbreaks. The experimental area is covered with dry savanna, scarce shrubby vegetation, and a few cultivated surfaces. The soil is almost flat with altitudes ranging from 200 to 250 m. This experiment has been thoroughly described in various papers (Druilhet and Tinga 1982; Druilhet and Durand 1984; Fouquart et al. 1987a). We shall give only a brief description of the ground and airborne data used in the present study. The ECLATS dataset contains no satellite data (*Meteosat-1* had a failure and *Meteosat-2* had not yet been launched).

1) SURFACE DATA

The site latitude and altitude are 14°N and 220 m, respectively. A surface station at the Niamey airport continuously recorded the soil surface temperature T_S, the surface heat flux density G, the wind speed (cup anemometers) and the air temperature at two levels (0.75 and 2.25 m), the downward shortwave $F_s\downarrow$, the longwave $F_l\downarrow$, and net F_n irradiances. The data were averaged over 20-min intervals. A two-level aerodynamic method (Itier 1980) provided the sensible heat flux H. The latent heat flux LE was derived from the surface energy budget equation: $H + \mathrm{LE} + G = F_n$. Two multiwavelength radiometers measured the optical thicknesses and the water vapor content. A cascade impactor was used to monitor aerosol concentration and size. Additional data were provided by the observation station of ASECNA (the Agence pour la Securité de la Navigation Aérienne, an office concentrating the meteorological services of most of the francophone African countries) at the Niamey airport: surface turbidity observations from horizontal visibility, hourly wind at 10 m, soil temperature at depths 10, 20, 50, and 100 cm at 0600, 1200, and 1800 LST.

2) AIRCRAFT AND BALLOON MEASUREMENTS

The wind, temperature, humidity, and aerosol size and concentration profiles were measured using an instrumented aircraft (HD-34 INAG-EDF). During the flights, the profiles of the irradiances (upward and downward, shortwave and longwave) were recorded. Moreover, ASECNA balloon soundings of temperature and humidity were available.

b. Comparison of model results with experiment

1) CHOICE OF TYPICAL CASES

In order to test the model under different conditions, we have selected data from three representative and well-documented days. The criteria were:

(i) cloudless sky (but thin high clouds could not be avoided and were taken into account in a somewhat rough way);

(ii) constancy in atmospheric dust content over the 24-h period (daily cycle from 0600 to 0600 LST the next day). This condition is naturally of prime necessity as our model deals with constant aerosol profiles only. This constancy was assumed from surface visibility observations, as visibility and optical thickness are closely related (Legrand et al. 1988);

(iii) aerosol concentrations as different as possible;

(iv) surface meteorological conditions (wind, temperature) as different as possible.

The three selected days are 21 and 26 November (days 7 and 12) and 8 December (day 24). Day 24 presents a weak turbidity: the spectral average of the shortwave optical thickness δ_s is 0.22. Day 12 is the most turbid with δ_s equal to 0.86. Day 7, with δ_s equal to 0.34, presents an intermediate value (Fouquart et al. 1987b).

As may be seen, this experiment provides as much data as we need for qualifying a model, but they are in no way sufficient to carry out a direct investigation without model.

2) MODEL INITIALIZATION

Simulations over 24 h begin at sunrise (0600 LST). The initial temperature, humidity, and aerosol profiles come from the aircraft sounding, whereas the wind profiles are derived from the 0500 LST pilot balloon soundings. The temperature profiles are likely to change only in the boundary layer, and very few variations are observed over 2000 m, so that the three initial profiles are similar above this level. The air humidity is almost constant over the day, and its effect on the energy exchanges is moderate. The total water vapor contents are only 1.49, 1.91, and 1.65 g cm^{-2}. The soil temperature profile is derived from the 0600 LST observations. The exact initial value of T_S is rather insignificant, as shown by the numerical tests: the calculated surface temperature converges toward the same values after a short simulated time. The aerosol profiles are derived from the inflight measurements and they are held constant over the day. The aerosol properties are derived from Fouquart et al. (1987a,b) and are summarized in Table 1. At the top of the domain, the wind vector, temperature, humidity, and aerosol are held constant over the whole 24-h run.

Surface constants listed in Table 2 were adjusted, using all available data. As most of these constants were not systematically measured, we have determined them by a tuning procedure, based upon a general agreement of model calculations with experimental data, provided that all the constants are realistic.

(i) Thermal ground properties (thermal diffusivity κ, density ρ, and specific heat C) have not been measured during ECLATS. A previous study (Cautenet et

TABLE 1. Values of the main constants describing the aerosol during the three test days: δ_s is the shortwave optical thickness, ω the single-scattering albedo, g the asymmetry factor, δ_s^c and δ_l^c, respectively, the shortwave and longwave optical thicknesses associated to cloud cover, σ_l the gray longwave absorption coefficient per particle, and S the solar flux at the top of the atmosphere.

	Day 7 (21 November 1980)	Day 12 (26 November 1980)	Day 24 (8 December 1980)
δ_s	0.34	0.86	0.22
ω	0.948	0.958	0.952
g	0.666	0.657	0.650
σ_l (cm^{-2})	5.80×10^{-2}	4.80×10^{-2}	1.80×10^{-2}
δ_l^c	0.55	0.50	0.60
σ_s^c	0.25	0.22	0.26
S (W m^{-2})	1387	1390	1395

al. 1986) allowed to ascribe a value of 1000 J K^{-1} m^{-2} s$^{-1/2}$ for the thermal inertia $I = \rho C \kappa^{1/2}$, a parameter that governs soil surface temperature, regardless of the values of ρ, C, and κ. After reaching a good agreement in surface temperature, we tuned ρC and κ until the inner computed temperatures agreed with the respective experimental values, whenever it was possible to compare (three times per day for ASECNA measurements). For all the days, the same values of ρC and κ, and therefore of I, were adopted: this is physically justified as no rainfall occurred during this period, which could have modified the thermal properties. The same can be said for all the surface properties.

(ii) The soil surface moisture m was not measured during ECLATS. In the model, this parameter is the relative humidity of the upper soil layers. The experimental values of latent heat flux were weak (diurnal values are generally under 30 W m^{-2}). A value of about 0.01 for m provides a good agreement of the model results with the experiment.

(iii) A value of 0.1 cm for the roughness length z_0 was selected. It may seem weak, but it should be reminded that vegetation was scarce in the area.

(iv) The radiative ground properties, surface albedo A and emissivity ϵ (both parameters averaged over all wavelengths and space directions), were equal to 0.26 and 0.90, respectively, and were also held constant. The albedo was determined from upward and downward shortwave irradiance measurements during flights at 100 ft above the ground. As the effect of the emissivity was not critical, a value usually reported in the literature has been ascribed.

An experimental determination of some ground properties of the experimental site was performed by Druilhet (1983) at the beginning of the rainy season following ECLATS (May 1981). The volumetric heat

TABLE 2. Values of the main surface constants: κ is the diffusivity, ρC the volumetric heat, I the thermal inertia, A and ϵ, respectively, the albedo and the emissivity, m the soil moisture, and z_0 the roughness length.

κ (m^2 s^{-1})	2×10^{-7}
ρC (J K^{-1} m^{-3})	2.24×10^6
I (J K^{-1} m^{-2} s$^{-1/2}$)	1000
A (global)	0.26
ϵ (global)	0.90
m	0.01
z_0 (cm)	0.10

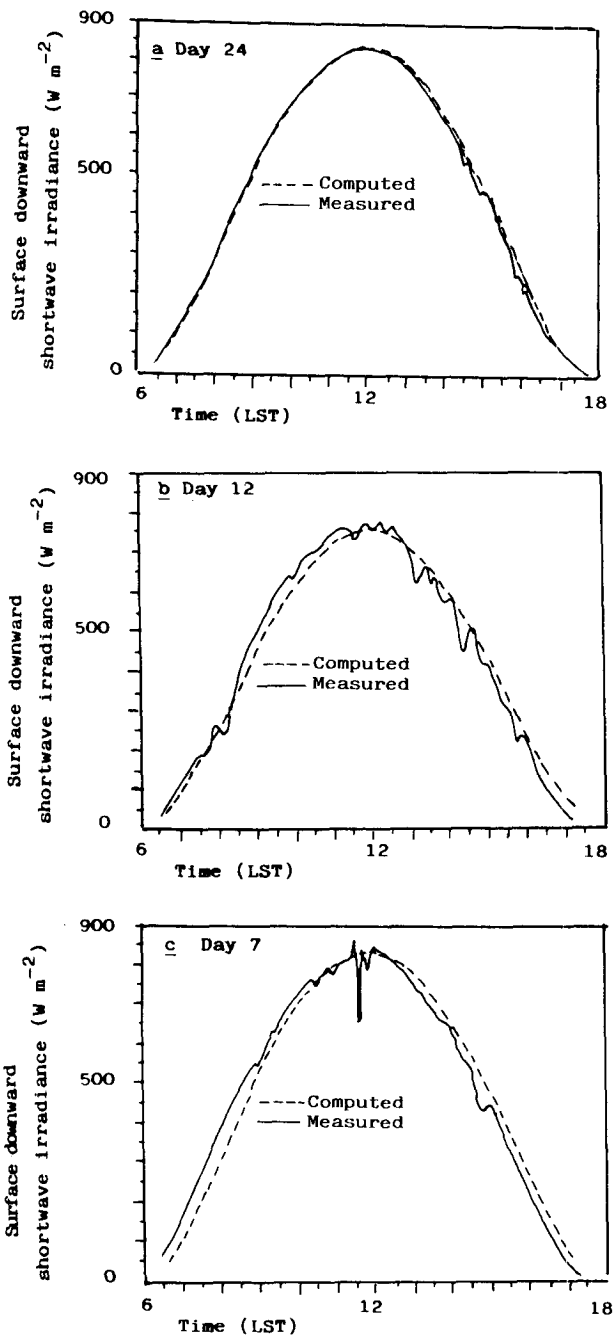

FIG. 1. Experimental (solid line) and computed (dashed line) daily cycle of downward shortwave irradiance; (a) day 24, (b) day 12, and (c) day 7.

ρC agrees with our value (2.17 10^6 J K^{-1} m^{-3}). The values of moisture m (about 0.02) and of thermal inertia I (1280 J K^{-1} m^{-2} $s^{-1/2}$) are somewhat higher.

3) Results and discussion

Hourly results from 24-h runs are displayed in order to compare the model simulations with the observations.

(i) *Shortwave solar radiation*

As mentioned above, the presence of an absorbing layer representing the high clouds has been assumed. The adjustment was performed by tuning the optical thickness $\delta_s{}^c$, so that the daily values of the downward shortwave irradiance $F_s\downarrow$ computed and measured at ground level were equal. It may be noticed that instantaneous agreement is also very satisfactory when the cloud cover is constant (day 24, Fig. 1a). Fluctuations around average value may also occur, as illustrated by Fig. 1b (day 12) and Fig. 1c (day 7), obviously because of cloud cover inhomogeneities. We may observe a systematic standard deviation (departure of model results from experimental data) ranging from 2% (day 24) to 5% (day 12) of the daily amplitude. This justifies the assumption of a constant daily cloud cover, but we must keep in mind that instantaneous discrepancies may be more important. Two examples of vertical profiles of shortwave downward irradiance $F_s\downarrow$ are presented in Fig. 2a (day 24, 1520 LST) and

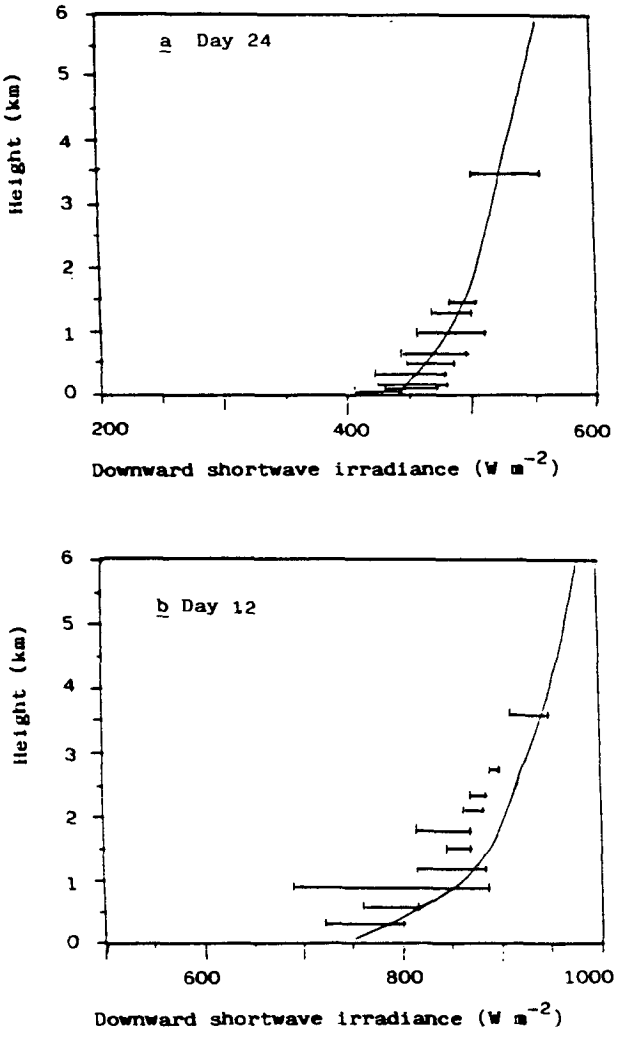

FIG. 2. Experimental (center of the horizontal bars) and computed (solid line) profiles of downward shortwave irradiance. Horizontal bars represent experimental scattering of measurements (and not an experimental error): (a) 1520 LST, day 24 and (b) 1100 LST, day 12.

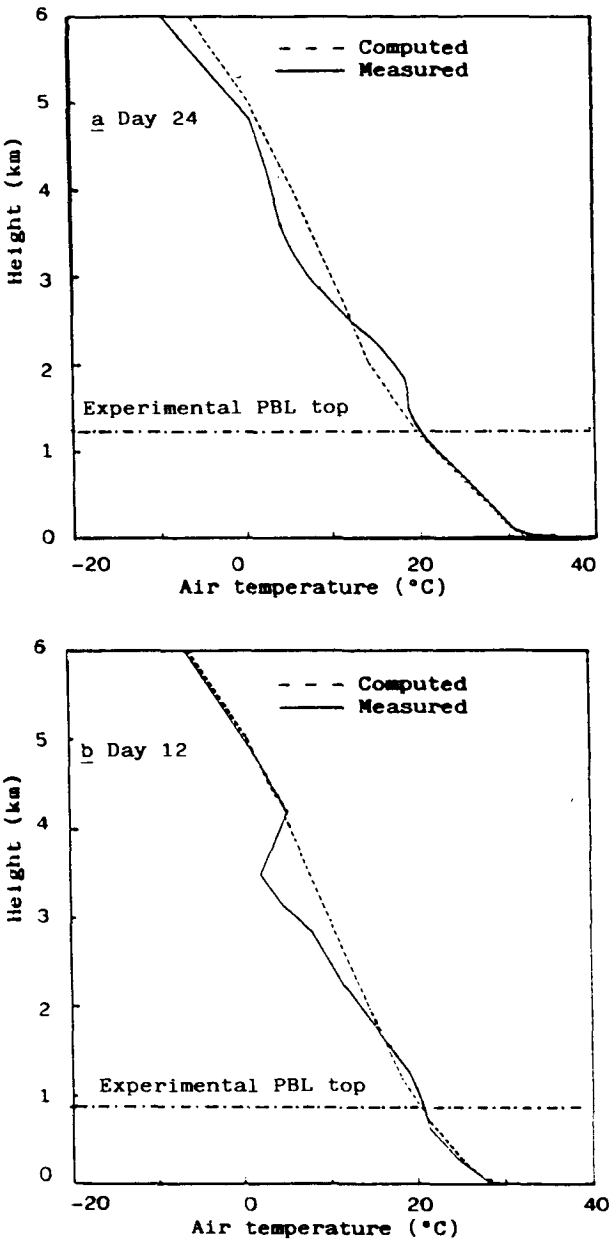

FIG. 3. Profiles of experimental (solid line) and computed (dashed line) air temperature: (a) 1520 LST, day 24; (b) 1100 LST, day 12.

in Fig. 2b (day 12, 1100 LST). In the second case, the calculations are slightly overestimated, chiefly between levels 1000 and 3000 m. The observed inverted vertical gradient of irradiance suggests that there could be a thicker cloud or a local dustiness increase in the investigated area. In fact, the examination of the surface global radiation (Fig. 1b) shows that the cloudiness was variable during the flight. The agreement seems more satisfactory on day 24. We may conclude that the calculations agree with the experimental aircraft data only when atmospheric inhomogeneities do not occur. As the model assumes that dustiness and cloud cover are uniform, of course, it cannot account for an irregular cloud or dust distribution.

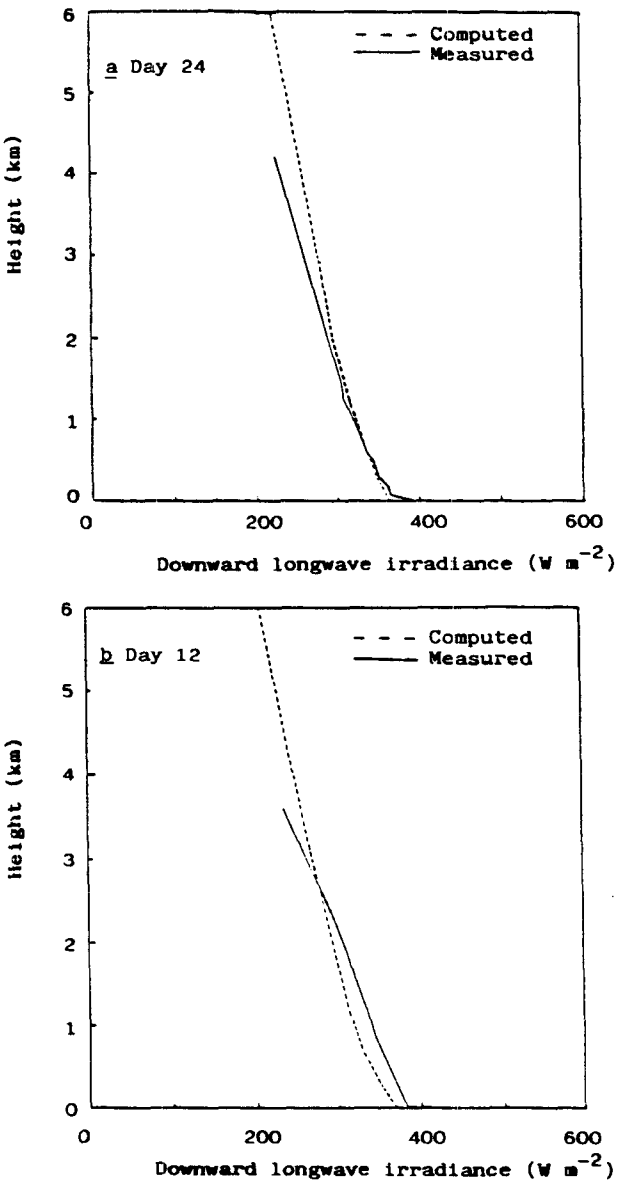

FIG. 4. Profiles of experimental (solid line) and computed (dashed line) downward longwave irradiance: (a) 1520 LST, day 24 and (b) 1100 LST, day 12.

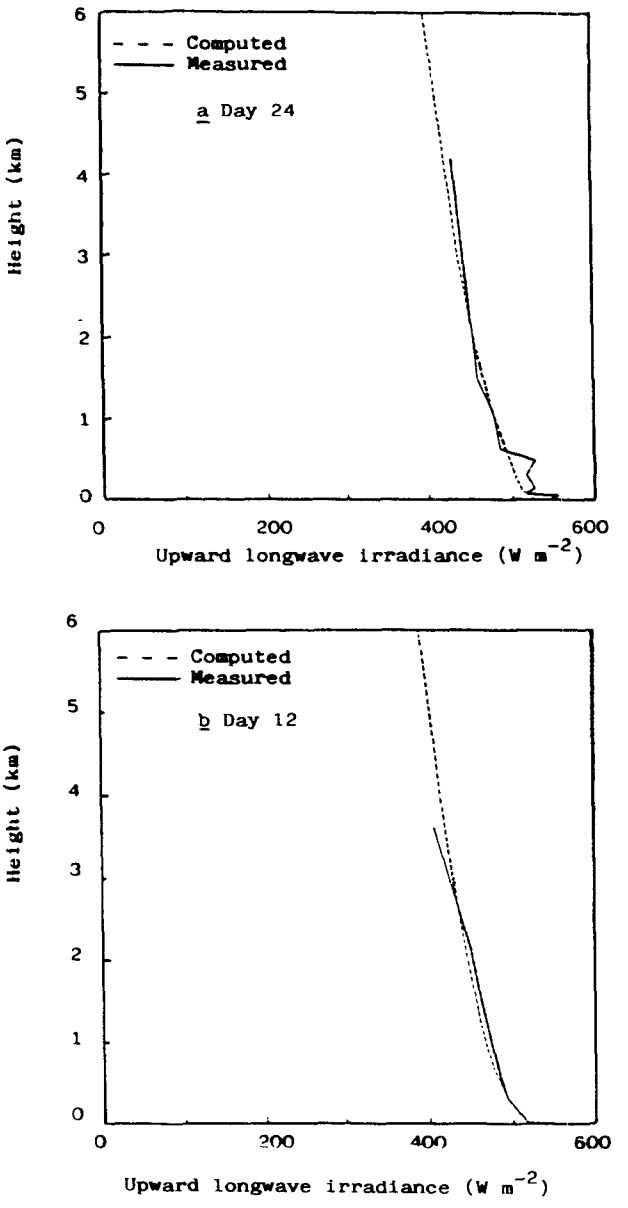

FIG. 5. Profiles of experimental (solid line) and computed (dashed line) upward longwave irradiance: (a) 1520 LST, day 24 and (b) 1100 LST, day 12.

Upward shortwave irradiance $F_s\uparrow$ was not examined here; although experimental data are available, large variations in their values arise from the surface albedo variability.

(ii) *Longwave radiation and temperature profiles*

Two examples are displayed: day 24 (lowest turbidity) and day 12 (highest turbidity). On day 24, Figs. 3a, 4a, and 5a are relative to temperature and longwave irradiance profiles (downward and upward) at 1520 LST; air temperature at 2 m above ground is presented in Fig. 6a. Figures 3b, 4b, 5b (profiles at 1100 LST), and 6b present the same parameters for day 12. The

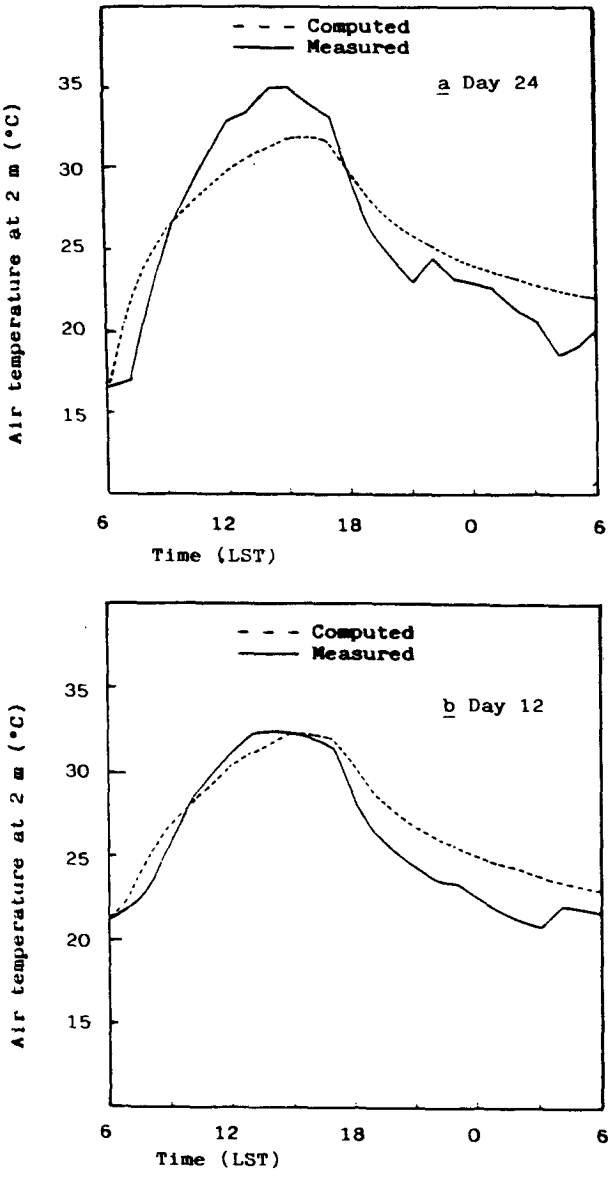

FIG. 6. Experimental (solid line) and computed (dashed line) daily cycles of air temperature at 2 m above ground: (a) day 24 and (b) day 12.

air temperature is generally satisfactory from 0 to 1500 m. Departures between experimental and calculated values range from 0 to 1°C between the surface layer and the top of the boundary layer (except on day 7 where they reach 2°C). Near the ground, where local influences may predominate, calculated temperatures are underestimated during daytime and overestimated during nighttime. We may observe a phase lag and an attenuation in amplitude of the calculated temperature diurnal variations.

Above the boundary layer (i.e., broadly speaking, above 1500–2000 m), departures are greater, particularly on day 12 around 3000 m, where an inversion layer of some 100 m is not captured by the model. This might be explained by synoptic movements such as large-scale ascent or subsidence, which are not taken into account because they are neither monitored by the model nor experimentally recorded. This discrepancy might also originate partly from some inaccuracy in the model heat fluxes. However, continuous experimental flux profiles are not available, so that no direct comparison can be performed. The aforementioned large-scale atmospheric motions are related to the intertropical convergence zone (ITCZ) movements. Nevertheless, these discrepancies are of minor importance, as the application, that is, the satellite response study, is thought to depend chiefly on surface exchanges. As a rule, model results (temperatures or irradiances) are smoother than experimental results.

The model estimates of upward longwave irradiance $F_l\uparrow$ agree well with those of the measured fluxes, in spite of experimental fluctuations in the first 500 m not encountered in the model on day 24. These fluctuations are not explained and could result from inhomogeneities in the soil surface characteristics. They are not observed on the other days. In downward longwave irradiance $F_l\downarrow$, an average underestimation of about 20 W m^{-2} exists on day 12 between 0 and 2000 m, which is of the same order of magnitude as the model error (discussed in section 2b). Such an error is not observed on day 24. It must be noted that experimental longwave flux measurement (especially airborne) uncertainties could be invoked to explain the observed discrepancies (Brogniez et al. 1986; see also the report WCP-93, 1984). In fact, some of these errors are clearly cut off by tuning δ_l^c. Hence, the tuned values of δ_l^c probably have to be considered as widely different from the real cloud infrared optical depth.

(iii) *Surface temperature and conduction flux*

The amplitude and phase of the calculated ground surface temperature satisfactorily agree with the experimental data (Figs. 7a–7c). The standard deviation ranges from 0.8° to 1.3°C, that is, 3%–6% of the daily amplitude. In our procedure based upon a partial tuning, we have looked for a fairly general agreement with the whole available ECLATS dataset, rather than a particularly close agreement with the exclusive ground surface temperature. Model temperatures are slightly underestimated, which could be explained by the following mechanism, invoked earlier by Cautenet et al. (1986). The ground thermal inertia and conductivity are strongly influenced by the liquid water content. As the ground water is held constant in the model, the aforementioned properties do not vary during the 24-h cycle. Physically, however, the thermal inertia could vary as a diurnal cycle of the ground water is expected to exist. During daytime, evaporation reduces the soil wetness near the surface, which is restored during nighttime by capillarity processes from the inner layers. In agreement with this hypothesis, Druilhet's

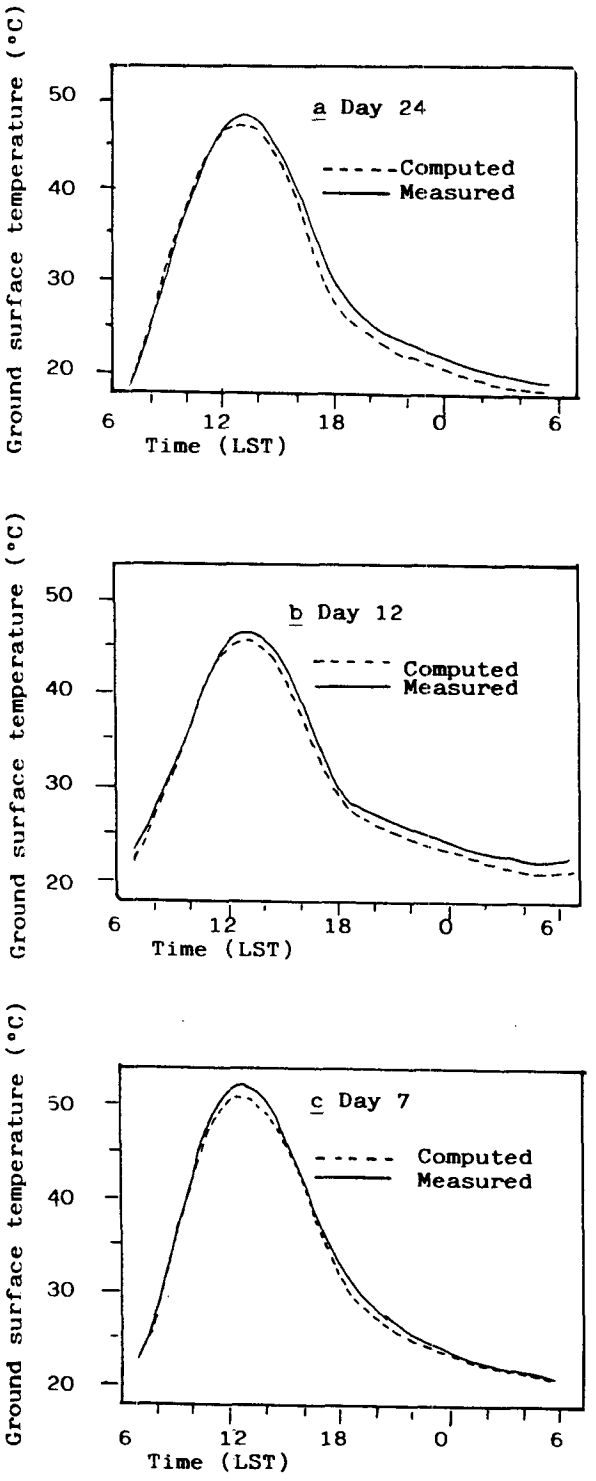

FIG. 7. Experimental (solid line) and computed (dashed line) daily cycles of ground surface temperature: (a) day 24, (b) day 12, and (c) day 7.

data (1983) showed that under 20 cm, humidity was about six times larger than at the ground surface. Hence, it could be hypothesized that actual daytime values of the thermal inertia are somewhat inferior to nighttime values. Thus, the former could be overestimated and the latter underestimated by the model. Now, sensitivity runs confirm that an increase in thermal inertia induces a nocturnal increase, and conversely a diurnal decrease of surface temperature. So, observed model underestimates of surface temperature could originate from the assumed constancy of the thermal inertia.

It can be noted that such a diurnal change could also affect noticeably the surface emissivity, as this parameter is also sensitive to the soil surface wetness.

Although an underestimation and a phase lag may be observed, the ground-conduction heat flux density G (Figs. 8a–8c) is, as a whole, correctly calculated. The departures between simulation and experiment may originate from the model, which approximates the ground-conduction heat flux density $G = -\lambda(\partial T/\partial z)_0$ by $G = -\lambda(T_S - T_1)/z_1$ (λ is the ground conductivity equal to $\kappa\rho C$, and T_1 the temperature at the first level z_1 under ground surface).

(iv) *Surface sensible and latent heat fluxes*

Owing to the soil surface dryness, the turbulent sensible heat flux H is much more important than the latent flux, which is not shown here. The calculated latent heat flux is about 10%–30% of the sensible flux, that is, it has the same order of magnitude as the experimental data. The experimental value of H is weak during nighttime (Figs. 9a–9c). It grows with surface temperature but, in the early afternoon, it decreases (collapses) rather quickly so that an asymmetry appears. On days 12 and 24, the calculated and experimental curves are in good agreement from sunset to noon. In the afternoon, the calculated curves do not present any collapse, so that the model overestimation prevails. On day 7, another phenomenon may be observed: the morning calculated value of H is weaker than the experimental value, and the experimental collapse occurs earlier than on the other days. At 0930 LST, the surface temperature already exceeds 43°C (on day 12, at the same time, it reaches 37°C, and 38°C on day 24). The Richardson number is as low as −3 and the air temperature gradient, between 75 and 225 cm, has its maximum value, say −0.9°C. At 1030 LST the H curve collapses and its value decreases from 240 to 140 W m^{-2} at 1100 LST. The absolute values of Richardson number and temperature gradient also decrease. The same occurrences may be observed on the two other days, with some differences: the collapse occurs around noon and its amplitude is fairly weaker, chiefly on day 12.

The collapse of the experimental curves seems to be a general feature during the ECLATS experiment, but it is particularly marked for days 7 and 24. In order to give a rough estimate of its importance, we have calculated the linear regression $H = aF_n + b$ between H and the surface net irradiance F_n. Before the collapse, the linear dependency is strong for the three days, with

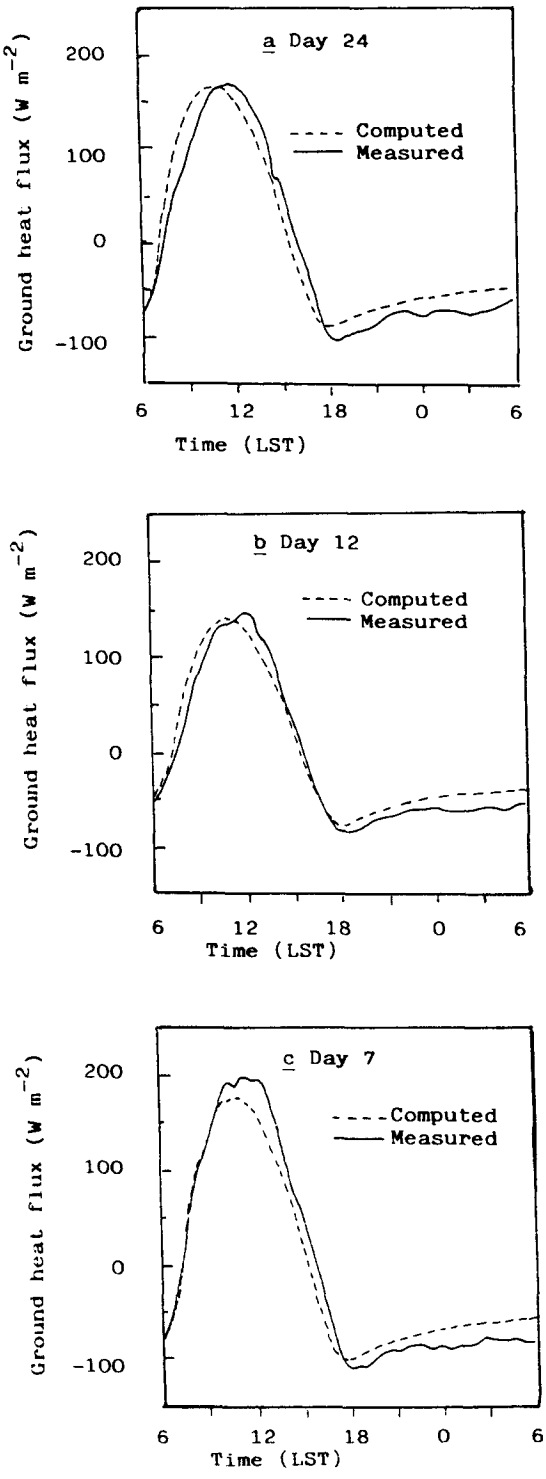

FIG. 8. Experimental (solid line) and computed (dashed line) daily cycles of ground surface conduction heat flux density: (a) day 24, (b) day 12, and (c) day 7.

a correlation coefficient r of about 0.96 or 0.97. After the collapse, r decreases: for instance, it is 0.97 before the collapse and 0.72 after on day 7. The corresponding values are 0.96 and 0.80 for day 24. On day 12, where the phenomenon is not strongly marked, the decrease of r is small (from 0.97 to 0.95). In every case, we observe a decrease of the coefficient a and an increase

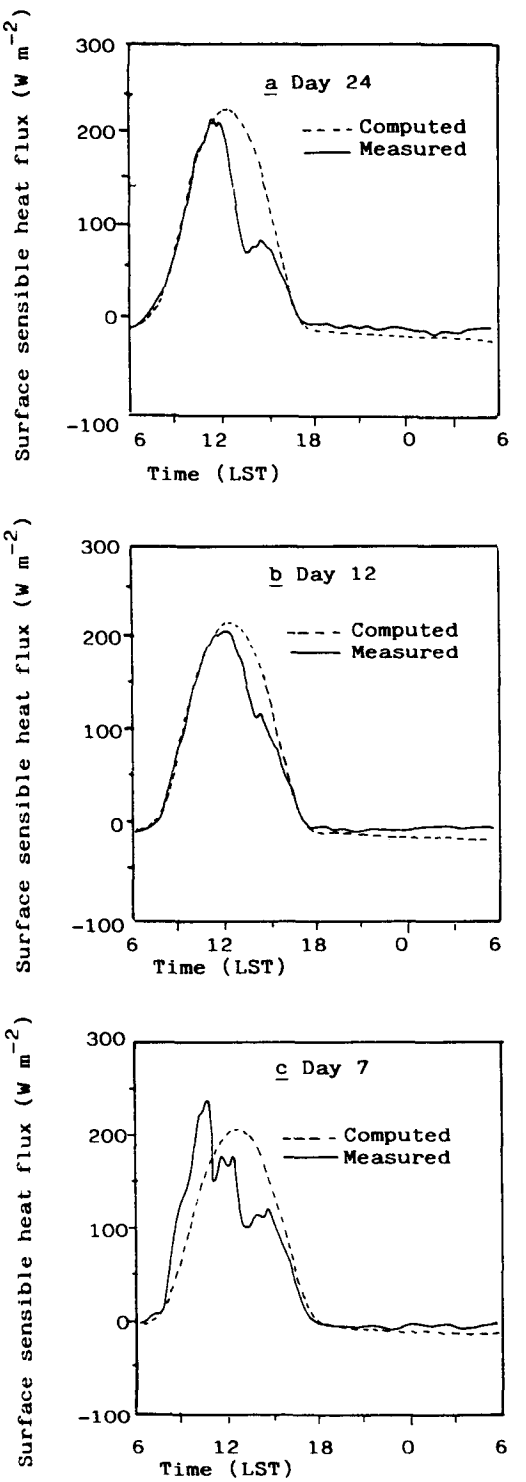

FIG. 9. Experimental (solid line) and computed (dashed line) daily cycles of surface sensible heat flux density: (a) day 24, (b) day 12, and (c) day 7.

of the intercept b, which changes from negative to positive. Using the morning regression, we can simulate roughly the shape of H that would exist if the collapse was not observed, so that the area of the collapse could be calculated. This area represents about 30% of the daily sensible energy on day 7, 1%–2% on day 12, and 7% on day 24. This last case corresponds roughly to the average value of the whole ECLATS period. The case of day 7 is exceptional.

What is the physical nature of this collapse? One may put forward two hypotheses. First, this phenomenon could be partly an artifact (Druilhet and Durand 1984) originating from the free convection conditions near the ground suggested by the large negative values of the Richardson number Ri. There is very scarce experimental information about the phenomenon of free convection in the atmosphere, but when wind is weak, the cup anemometers are likely to fail because their response is strongly influenced by local whirlwinds. Under these conditions, it can be hypothesized that the measured average vertical wind gradient overestimates the true value, so that the experimental value of H could be somewhat underestimated.

However, this phenomenon is certainly not completely artificial. Durand (1983) reports that in a few cases (4 in 15 flights) the airborne measured sensible heat flux increases with the height; among them, we find days 7 and 24. Under strongly superadiabatic conditions, a local free convection regime may occur near the ground with a lesser efficiency in the heat turbulent transfer, which could partly explain the collapsed shape of the curve. There must therefore be some compensatory mechanism that explains the PBL deepening. It can be hypothesized that this supply is of radiative nature. Intensity of the radiative supply in the longwave domain has been estimated using a spectral high-resolution model (Durand et al. 1988; Pagès et al. 1988): under superadiabatic conditions, the incoming longwave irradiance divergence typically amounts to 30 W m^{-2} in the 0–10-m layer and 60 W m^{-2} in the 0–100-m layer. However, direct measurement of sensible heat flux divergence in the surface layer is extremely difficult and has never been satisfactorily achieved. The consequence is that the surface universal functions used in modeling are not designed for these extreme conditions: as a matter of fact, as stated by Pagès et al. (1988), if energy supply is likely to exist in this layer, the classical universal functions based upon an absence of divergence in surface layer fluxes are, strictly speaking, no longer consistent. Moreover, the radiative supply depends upon superadiabatism ΔT and altitude z, whereas the universal functions depend on z/L (L is the Monin–Obukhov length). The extension to very unstable conditions of the surface-layer parameterization using stability functions is not completely satisfactory, so that the model is expected to be less efficient. In fact, it is just what we observed above. Fortunately, a statistical study of the daily Richardson number Ri shows that values as low as those observed on day 7 are exceptional: Ri decreases under -1 in four cases only between 18 November and 8 December, and for very short periods (except in the case of day 7). The more frequent daily values range from -0.1 to -0.3. The probability for Ri to become inferior to -0.5 is only 10%.

It can be concluded that comparison of model values of H with experimental data is not easy during the early afternoon period, where we notice obvious discrepancies, rather difficult to explain thoroughly. However, the model issues seem globally realistic because these discrepancies are likely to be severe only in a few cases.

(v) *Boundary-layer height*

As the sensible heat flux is a part (along with the radiative fluxes) of the source of the boundary-layer growth, one may wonder how the observed departures influence the PBL deepening. We can compare the calculated PBL height with the experimental one at time of the flight. In the model, the PBL height h_i is calculated following the prognostic Deardorff's (1974) formula and it represents the level at which the sensible heat flux is minimum. This theoretical formula is included in the model under the following hypotheses: horizontal homogeneity, no advection, no entrainment, and no synoptic-scale vertical movements (ascent or subsidence). On the other hand, the experimental values of h_i coincide with the determination by aircraft of the base of the first temperature inversion layer. As pointed out by Durand (1983), this definition is more convenient on an experimental basis, as the level of the minimum sensible flux is not easy to determine. Statistically, both definitions are equivalent. Experimental and calculated values may be fairly different because spatial inhomogeneities, local entrainment zones, and large-scale movements may modify this level rather strongly. However, this procedure is the only one we can use. Model results corresponding to time of the flight are 1500 m (day 7), 1000 m (day 12), and 1400 m (day 24), whereas respective experimental values (Durand 1983) are 2000, 900, and 1300 m. The model issue for day 7 is underestimated, which is related to the abovementioned remarks, whereas days 12 and 24 are in better agreement (slight overestimation).

(vi) *Surface net irradiance*

The net irradiance F_n (SW + LW) from the model is more regular than the experimental one but agrees well with it (Figs. 10a–10c). Rapid fluctuations are observed in Fig. 10b (and Fig. 10c also), indicating that the cloud cover is not perfectly homogeneous, the term of the downward shortwave irradiance being responsible of the fast variations, as may be seen when compared with the curves of Fig. 1a and Fig. 1b. The slight model overestimation partly results from the

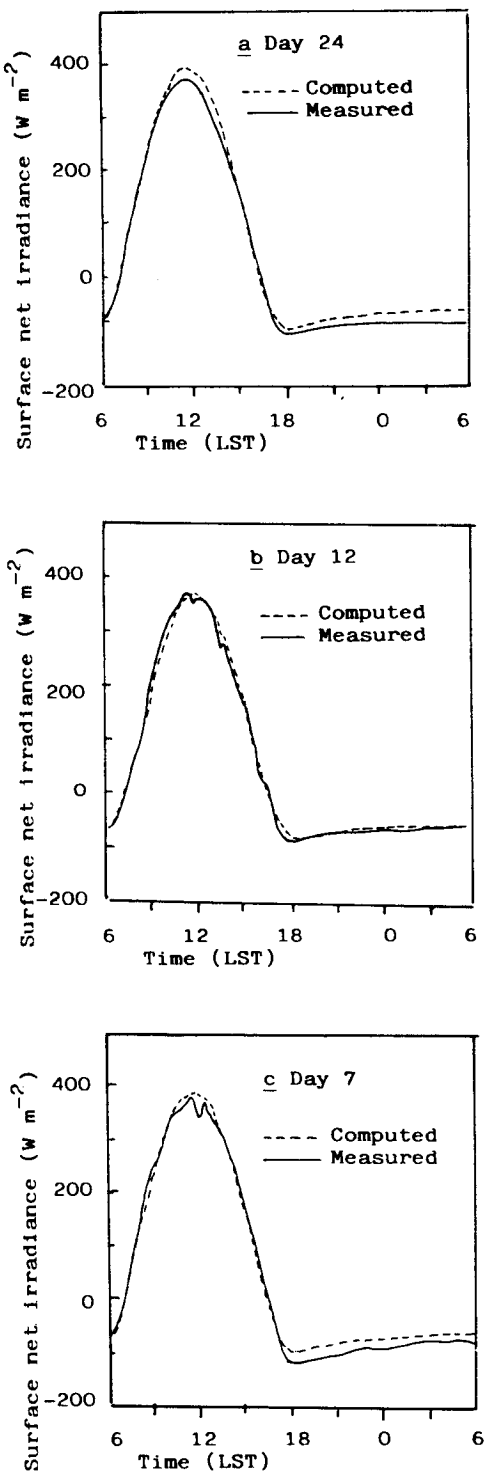

FIG. 10. Experimental (solid line) and computed (dashed line) daily cycles of surface net irradiance: (a) day 24, (b) day 12, and (c) day 7.

aforementioned underestimate in surface temperature. The standard deviation ranges from 14 to 18 W m^{-2}, while the temperature underestimate contributes for 5–8 W m^{-2}. When compared with the typical daily amplitude of 450–500 W m^{-2}, the relative value of this deviation is weak as it does not exceed 3%–4%.

It is noteworthy that during daytime the contribution of the turbulent heat fluxes amounts to half of the net irradiance, and about 30%–40% of the surface upward longwave irradiance (not shown here). The surface conduction heat flux ranges from 30% to 50% of the net irradiance. During the stable nocturnal period, a weak, negative (in the ground) sensible flux exists, but the main feature is a quasi balance between net radiation and ground-conductive heat flux. These experimental features are corroborated by model calculations.

Owing to the great relative weight of the turbulent and conduction fluxes in the surface energy budget, it is obviously necessary to take them into account to perform any realistic simulation of the radiative processes, and particularly of the infrared emission setting at the ground surface.

(vii) *Humidity*

In the three cases under study, the variations of this parameter are very weak over the 24-h period, in the experiment as well as in the model. At a level of 2 m, these variations range from 10% to 15% of the average value, and at upper levels variations are still weaker. This may be explained by the absence of water vapor advection (it may be noted that this quasi constancy during the day exists at a larger time scale: the water vapor contents are not very different in the three cases; see section 3b.2). Due to this quasi constancy and to the inaccuracy in humidity measurements, it would not be realistic to compare model issues with experimental data.

(viii) *Wind*

The wind is obviously the least satisfactory parameter of the model issues. We limit our discussion to the surface wind, since the wind profile, unlike the temperature profile, has no direct influence on the surface energy fluxes. Figures 11a–11c describe the surface wind speed as measured by the ground station at a level of 2.25 m (solid line) and the ASECNA station at a level of 10 m (dashed line with dots), and calculated by the model at 2 m (dashed line). Both experimental curves show large fluctuations. The zero values from the ASECNA station are due to the technique of wind recording: instantaneous values are read every hour so that a zero wind speed may appear. Moreover, the ASECNA anemometer is located 10 m above the ground, whereas the ground-station anemometer is located at the 2.25-m level, which explains that the ASECNA values are greater. Thus, we compare the 2.25-m measurements with model issues at 2 m. The phase behavior of the calculated wind is rather realistic: on day 7 (Fig. 11c), the slow increase from sunrise to 1700 LST on experimental record may also be observed

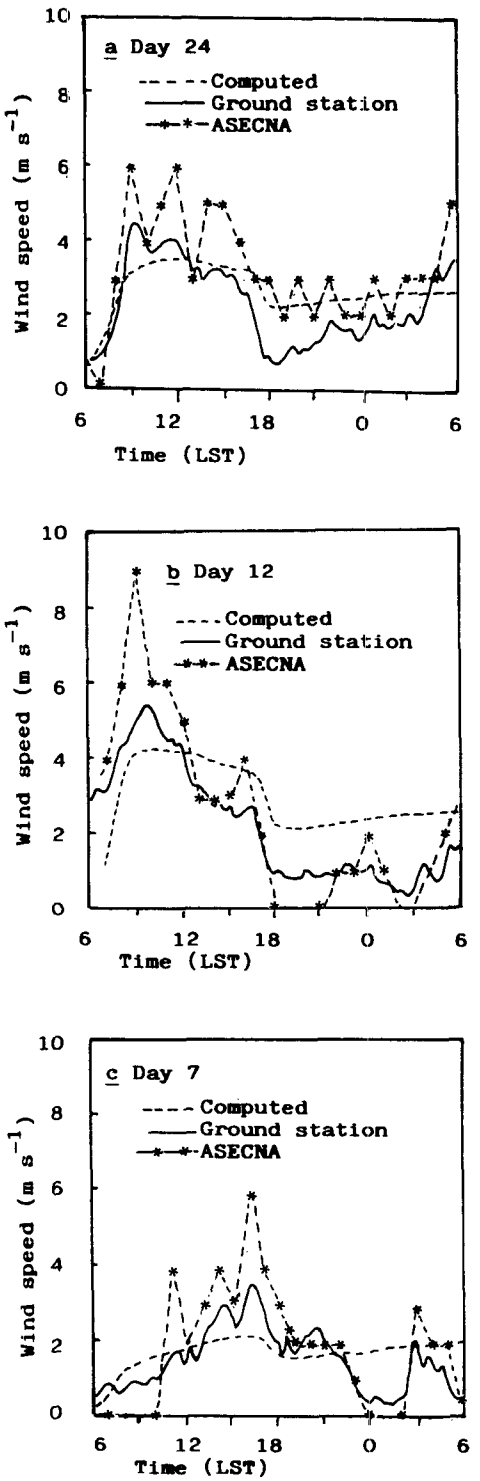

FIG. 11. Comparison of experimental wind measured by ground station (solid line) with computed wind (dashed line). In addition, wind at 10 m above ground (-- * -- * --) measured by the ASECNA station is presented; (a) day 24, (b) day 12, and (c) day 7.

on the calculated curve. The decrease at sunset also appears in experimental and calculated winds, but the nighttime calm between midnight and 0200 LST does not exist in the model. On the other two days (Figs. 11a and 11b), the experimental curves are somewhat different from those of day 7, as the morning wind increase is very fast now. The model results agree with the general shape of the experimental wind. Nevertheless, it is obvious that calculated and experimental data are fairly different. The calculated amplitudes are far smoother than the recorded ones. As stated by Pielke and Mahrer (1975), the inability of the model to perform an exact prediction of the wind results from neglecting factors such as advection and other disturbances, about which little information was available. Large-scale variations are governed in the model by a constant wind vector at the domain top and the vertical exchanges induced by the slow movement of the sun.

Near the ground surface, the thermal stratification issued from the model is not very realistic, as may be seen in the temperature curves. These differences in thermal stratification might be connected to the smoother shape of the calculated wind. As a matter of fact, we cannot expect to retrieve a complete description of the wind. We have already noted that the wind flow near the ground is strongly marked by whirlwinds around noon, so the cup anemometer's response could be somewhat erroneous. Rapid fluctuations originating from free convection could hardly be described by this model because, as stated above, it is not intended for a description of such a phenomenon, which would involve a special parameterization. The vertical scales, such as the free convective velocity scale w^*, are more likely to play a prominent role than the horizontal scales such as the friction velocity u^*.

In the morning, the increase in surface wind is somewhat greater in the experiment than in the model: the simulated low-level jet (LLJ) is smoothed. Although this phenomenon has little effect on the surface fluxes, it must be explained that LLJ simulation should need another model version. Following current theory, LLJ consists of an inertial oscillation of the extrageostrophic wind component near the ground, and is strongly influenced by such factors as baroclinity or vertical shear and variations in time of the geostrophic wind (see, for instance, Wipperman 1973 or Zeman 1979). In our model, the barotropy is assumed and the geostrophic wind shear within the PBL is not taken into account. Moreover, hourly measurements of the synoptic pressure field should be available to ensure a good simulation of the LLJ.

There remains the fact that the smooth shape of the model wind is probably not very realistic. Fortunately, it is commonly acknowledged that the surface fluxes are not very sensitive to the wind accuracy. For instance, under similar meteorological conditions (Niamey, dry season), a surface energy exchange model showed that a variation of ±25% in the wind speed led to an opposite variation inferior to 1°C in the surface temperature maximum, no variation in the minimum, and average energy fluxes almost unmodified (Cautenet 1987). It must be noted, however, that such a model

does not provide a completely realistic scheme as feedbacks are not accounted for: in a surface model, the surface wind is an external forcing factor, as well as the air temperature, humidity, and surface incoming radiation. The variation of the forcing factors is by no means influenced by the surface fluxes. Conversely, in our present model, such feedbacks are considered, which could a priori change the results. So it was necessary to verify this assumption. It seems that we have actually a rather weak dependence of the fluxes on the surface wind. For this reason, the observed discrepancies are not really prejudicial to the accuracy of the other issues, explaining that a general agreement exists between the model and the experiment.

4. Conclusion

The aim of Part I is to verify a model able to describe the aerosol effect in Sahelian conditions. This model will achieve sensitivity tests of infrared satellite response to atmospheric dust content, since the lack of experimental data precludes any direct study. The most important parameter for the satellite response is the ground surface temperature; therefore, the model has to estimate this temperature as accurately as possible. Numerical tests are performed for periods not longer than 24 h, in order to minimize the effect of large-scale slow variations. Tested situations are well documented and describe various meteorological conditions, including large differences in dust content. In fact, the tests showed that the calculated surface temperatures are closely similar to the experimental data, with a standard error of about 1°C. The surface fluxes, which are strongly dependent on the surface temperature, are also satisfactorily retrieved, except for discrepancies observed on the sensible heat flux. This sensible heat flux amounts to about half of the net irradiance and 30%–40% of the upward surface irradiance, both in the model and the experiment. The conduction heat flux is also far from being negligible. The profiles of irradiances are realistic. On the other hand, the wind is poorly estimated by the model; only the general shape of the surface wind speed has been reproduced. Fortunately, the wind influence upon the surface temperature is rather small, which affirms that a number of the model issues are satisfactorily calculated. These results prove that a simulation of radiative processes absolutely requires that nonradiative processes be taken into account.

We may conclude that the present model is a satisfactory tool to supply for the lack of experimental data and is suitable to the providing of numerical experiments, as will be carried out in Part II.

Acknowledgments. The authors gratefully thank Professor R. A. Pielke of Colorado State University for the mesoscale model. They also wish to thank Dr. Druilhet, who provided them with the surface data, and ASECNA for the ground and sounding data. They are indebted to CIRCI (numerical center of Abidjan, Côte d'Ivoire) and to the IBM board at Abidjan for their support in numerical work achievement.

REFERENCES

Brinkman, A. W., and J. McGregor, 1983: Solar radiation in dense Saharan aerosol in Northern Nigeria. *Quart. J. Roy. Meteor. Soc.*, **109**, 831–847.

Brogniez, G., J. C. Buriez, J. C. Vanhoutte, and Y. Fouquart, 1986: An improvement of the calibration of the Eppley pyrgeometer for the case of airborne measurements. *Beitr. Phys. Atmos.*, **59**, 538–551.

Cautenet, G., 1987: Possibilités et limites d'utilisation de l'équation du bilan d'énergie pour la détermination des échanges au sol en zone tropicale avec des données de routine. *Thèse de Doctorat d'Etat de Sciences Physiques* N° 392, Université de Clermont II, France, 234 pp.

——, M. Legrand, Y. Coulibaly, and Ch. Boutin, 1986: Computation of ground surface conduction heat flux by Fourier analysis of surface temperature. *J. Climate Appl. Meteor.*, **25**, 278–283.

Cautenet, S., and R. Rosset, 1989: Numerical simulation of sea breeze with vertical wind shear during dry season at Cape of Three Points, West Africa. *Mon. Wea. Rev.*, **117**, 329–339.

Cerf, A., 1985: Contribution à l'étude des aérosols sahariens: influence sur le transfert du rayonnement dans l'atmosphère, caractéristiques optiques. *Thèse de Doctorat d'Etat de Sciences Physiques,* N° 623, Université des Sciences et Techniques de Lille, France, 281 pp.

Coakley, J. A., and R. Cess, 1985: Response of the NCAR community climate model to the radiative forcing by the naturally occurring tropospheric aerosol. *J. Atmos. Sci.*, **42**, 1677–1692.

D'Almeida, G. A., 1986: A model for Saharan dust transport. *J. Climate Appl. Meteor.*, **25**, 903–916.

Deardorff, J. W., 1974: Three-dimensional numerical study of the height and mean structure of a heated planetary boundary layer. *Bound.-Layer Meteor.*, **7**, 81–106.

Druilhet, A., 1983: Etude expérimentale de la couche de surface sahélienne. *Rapport Interne N°1-1983.* Laboratoire d'Aérologie, Université Paul-Sabatier, Toulouse, France, 31 pp.

——, and A. Tinga, 1982: Présentation de l'expérience ECLATS. *La Météorologie,* **29–30**, 203–212.

——, and P. Durand, 1984: Etude de la couche limite convective sahélienne en présence de brumes sèches (expérience ECLATS). *Bound.-Layer Meteor.*, **28**, 61–77.

Durand, P., 1983: Etude de la couche-limite convective sahélienne en présence de brumes sèches (expérience ECLATS). *Thèse de Docteur-Ingénieur* N°826, Université Paul-Sabatier, Toulouse, France, 165 pp.

——, J. P. Frangi, and A. Druilhet, 1988: Energy budget for the sahel surface layer during the ECLATS experiment. *Bound.-Layer Meteor.*, **42**, 27–42.

Fouquart, Y., and B. Bonnel, 1980: Computations of solar heating of the Earth's atmosphere: A new parameterization. *Beitr. Phys. Atmos.*, **53**, 35–62.

——, ——, M. Chaoui Roquaï, R. Santer, and A. Cerf, 1987a: Observations of Saharan aerosols: Results of ECLATS field experiment. Part I: Optical thickness and aerosol size distributions. *J. Climate Appl. Meteor.*, **26**, 28–37.

——, ——, G. Brogniez, J. C. Buriez, L. Smith, J. J. Morcrette, and A. Cerf, 1987b: Observations of Saharan aerosols: Results of ECLATS field experiment. Part II: Broadband radiative characteristics of the aerosols and vertical radiative divergence. *J. Climate Appl. Meteor.*, **26**, 38–52.

——, ——, and V. Ramaswamy, 1991: Intercomparing shortwave radiation codes for climate studies. *J. Geophys. Res.*, **96**, 8955–8968.

Fravalo, C., Y. Fouquart, and R. Rosset, 1981: The sensitivity of a model of low stratiform clouds to radiation. *J. Atmos. Sci.*, **38**, 1049–1062.

Itier, B., 1980: Une méthode simplifiée pour la mesure du flux de chaleur sensible. *J. Rech. Atmos.*, **14**, 17–34.

Joseph, J. H., 1977: The effect of desert aerosol on a model of the general circulation. *Proc. Symp. on Radiation in the Atmosphere,* H. J. Bolle, Ed., Science Press, 487–492.

Legrand, M., M. Desbois, and K. Vovor, 1988: Satellite detection of Saharan dust: Optimized imaging during nighttime. *J. Climate,* **1,** 256–264.

——, G. Cautenet, and J. C. Buriez, 1992: Thermal impact of Saharan dust over land. Part II: Application to satellite IR remote sensing *J. Appl. Meteor.,* **31,** 181–193.

Lenoble, J., 1984: A general survey of the problem of aerosol climatic impact. *Aerosol and their Climatic Effects,* H. E. Gerber and A. Deepak, Eds., A. Deepak Publishing, 279–293.

Mahrer, Y., and R. A. Pielke, 1978: A test of an upstream spline interpolation technique for the advective terms in a numerical mesoscale model. *Mon. Wea. Rev.,* **106,** 818–830.

Pagès, J. P., J. P. Frangi, P. Durand, Cl. Estournel, and A. Druilhet, 1988: Etude de la couche limite de surface sahélienne: Expérience Yantala. *Bound.-Layer Meteor.,* **43,** 183–203.

Pielke, R. A., and Y. Mahrer, 1975: Representation of the heated planetary boundary layer in mesoscale models with coarse vertical resolution. *J. Atmos. Sci.,* **32,** 2288–2308.

Tanré, D., and M. Legrand, 1991: On the satellite retrieval of Saharan dust optical thickness over land: Two different approaches. *J. Geophys. Res.,* **96,** 5221–5227.

——, J. F. Geleyn, and J. Slingo, 1984: First results of the introduction of an advanced aerosol–radiation interaction in the ECMWF low resolution global model. *Aerosol and their Climatic Effects,* H. E. Gerber and A. Deepak, Eds., A. Deepak Publishing, 133–177.

WCP, 1984: The intercomparison of radiation codes for climate models: Longwave clear-sky calculations. F. M. Luther, Ed., WCP-93.

Wipperman, F., 1973: Numerical study on the effects controlling the low-level jet. *Beitr. Phys. Atmos.,* **46,** 137–154.

Zeman, O., 1979: Parameterization of the dynamics of stable boundary layers and nocturnal jets. *J. Atmos. Sci.,* **36,** 792–804.